Ferroelectricity and Pressure-Induced Phenomena Driven by Neutral Ionic Valence Instability of Acid–Base Supramolecules

Reiji Kumai,*[†,‡] Sachio Horiuchi,[‡,§] Jun Fujioka,[⊥,∥] and Yoshinori Tokura[‡,⊥,∥]

[†]Condensed Matter Research Center (CMRC) and Photon Factory, High Energy Accelerator Research Organization (KEK), Institute of Materials Structure Science, Tsukuba, 305-0801, Japan
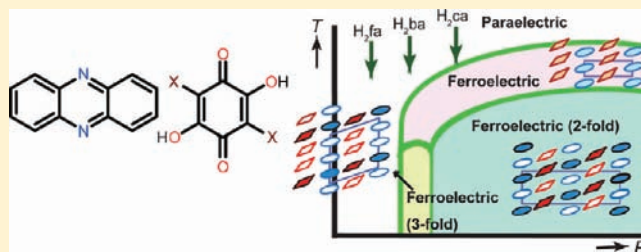
[‡]National Institute of Advanced Industrial Science and Technology (AIST), Tsukuba, 305-8562, Japan

[§]CREST, Japan Science and Technology Agency (JST), Tokyo 102-0075, Japan

[⊥]Department of Applied Physics, The University of Tokyo, Tokyo 113-8656, Japan

[∥]Correlated Electron Research Group (CERG) and Cross-Correlated Materials Research Group (CMRG), RIKEN Advanced Science Institute, Wako 351-0198, Japan

ABSTRACT: Supramolecular ferroelectric cocrystals of phenazine (Phz) with chloranilic acid (H_2ca), bromanilic acid (H_2ba), and fluoranilic acid (H_2fa) have been characterized by the interplay between their structural transformations and solid-state acid–base (proton transfer) reactions. At ambient pressure, the Phz-H_2ca, Phz-H_2ba, and their deuterated crystals exhibit incomplete proton displacement, which transforms the neutral molecules into semi-ionic at low temperatures below the Curie point ($T_c^{IC} < T < T_c^{I}$). For the cocrystal of the less acidic H_2fa, the ferroelectric phase is induced only by applying hydrostatic pressure above ~0.6 GPa. According to the combined studies of temperature-dependent dielectric permittivity and synchrotron X-ray diffraction, it was proved that the ferroelectric (FE-I) phase is always accompanied at lower temperatures by successive phase transitions to the lattice modulated phases with incommensurate periodicities (IC phase, $T_c^{II} < T < T_c^{IC}$) and with commensurate (2- or 3-fold) periodicities (FE-II or FE-III phase, $T < T_c^{II}$). Whereas the ground-state structures at ambient pressure are different from one another among the Phz-H_2ca (FE-II form), Phz-H_2ba (FE-III form), and Phz-H_2fa (paraelectric form), their systematic changes under pressure depict a universal pressure–temperature phase diagram. The possible origins of structural changes are assigned to the valence instability and the frustrated Coulomb interactions that induce the charge disproportionation (coexisting neutral ionic) states with the staging spatial orders.

1. INTRODUCTION

Charge redistribution from neutral crystalline solids under external stimuli has long been an attractive issue of solid-state science. For instance, the boron has turned out to be the first element whose solid becomes partially ionic (γ-B_{28} phase) through charge disproportion into a negatively charged B_{12} cluster and a positively charged B_2 unit under compression.[1] Similarly for the molecular hydrogen under ultrahigh pressure, the first-principles calculations have predicted the development of ionic character toward protonium hydride (H^+H^-) with emerging spontaneous polarization instead of the long-expected metallic state of dense hydrogen solids.[2] The theoretical calculations have also predicted proton-disproportionate ionic $NH_4^+NH_2^-$ forms for the ammonia solid due to the electrostatic energy gain under dense packing.[3]

The charge disproportionation has been still a rare case among single-component molecular solids. For instance, the 4,6-dihydroxy-pyrimidine molecule reveals the polymorphism yielding both a neutral molecular form and a proton-disproportionate ionic form of protonated cation and deprotonated anion, although these two polym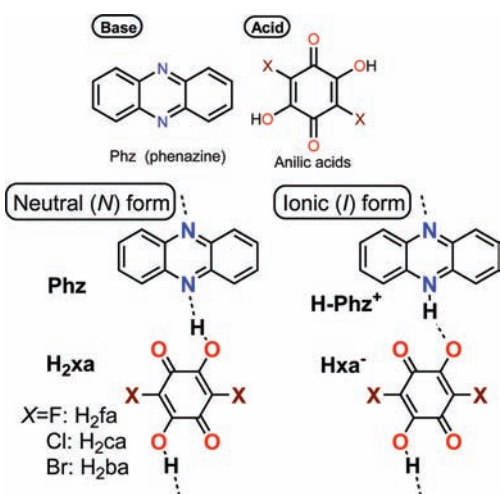orphs have not been interchanged with each other.[4] In contrast, the charge degree of freedom is more flexible on binary component molecular systems called charge-transfer (CT) complexes. Alternately π-stacked electron donor (D) and acceptor (A) molecules can be transformed from neutral to ionic form under moderate stimuli, like temperature variation and modest hydrostatic pressure, which modify the Coulombic attractive gain of ionized lattice and then energy balance relative to the cost of ionization (i.e., difference between the ionization energy of D and electron affinity of A).[5−7] Such a neutral ionic (NI) phase transition has been attracting interest also from the viewpoint of ultrafast photoinduced phenomena.[8,9]

Recently, NI valence instability has been differently perceived on some acid–base supramolecular ferroelectrics.[10] In the neutral cocrystals of hydrogen-bonded phenazine (Phz, proton acceptor, A) and anilic acid (H_2xa, donor, D) (Scheme 1),[11] ferroelectricity is realized from the chloranilic acid (H_2ca, X = Cl) and bromanilic acid (H_2ba, X = Br) but not from the less proton-donating fluoranilic

Scheme 1. Chemical Structures of the Neutral and Ionic Hydrogen Bonds Between Phz and H_2xa Molecules

acid (H_2fa, X = F).[12] The paraelectric phase structure comprises the nonpolar neutral molecules, which strengthen the partially ionic character below the Curie point T_c^I; the H_2xa releases one of the two protons toward the center position between the O and N atoms for a spontaneous asymmetrization.[13]

In analogy to the NI transition of CT complexes,[5−7] the cost of ionization of an acid−base pair is interpreted in terms of that of proton transfer relevant to the proton affinities or acidic equilibrium constants pK_a of D and A molecules. Indeed, the pK_a values are nearly matched between the Phz (1.20) and H_2ca (0.73) or H_2ba (0.80)[14,15] and could minimize the energy difference between the neutral and proton-transferred ionic forms. Meanwhile, contraction of the ionic crystal lattice under hydrostatic pressure would effectively gain the electrostatic energy term.

Here we report on systematic changes of the dielectric and structural properties of the series of Phz-H_2xa as a function of temperature (T) and hydrostatic pressure (p). In view of previous studies at ambient pressure, the Phz-H_2ca, Phz-H_2ba, and Phz-H_2fa crystals are distinct from one another in terms of the ground-state structure and ionicity. All these crystals under compression exhibited a complicated temperature dependence of permittivity indicative of successive structural phase transitions. In this study, we have unraveled the whole systematics of the respective dielectric/superstructure phase by probing the wide temperature−pressure region. Furthermore the synchrotron X-ray diffractions from single crystals have been examined to identify each structural phase. Through the finding of a universal pressure−temperature phase diagram, we show that the structural and ionicity changes during the ferroelectric and related phase transitions can be consistently interrelated to the effects of electrostatic intermolecular interactions under temperature- or pressure-induced lattice contraction.

2. EXPERIMENTAL SECTION

2.1. Materials. The single crystals of Phz-H_2xa (X = Cl, Br, and F) and deuterated Phz-D_2ba were grown according to the procedures reported previously.[12,16]

2.2. Dielectric Measurements. Measurements of dielectric constant using an LCR meter (HP 4284A) were done on the single crystals with gold or silver paste painted as the electrodes. Hydrostatic pressure was generated in a clamp-type high-pressure cell using the pressure-transmitting oil (Idemitsu Kosan Daphne 7373). The applied pressure at each transition point was obtained by correcting the
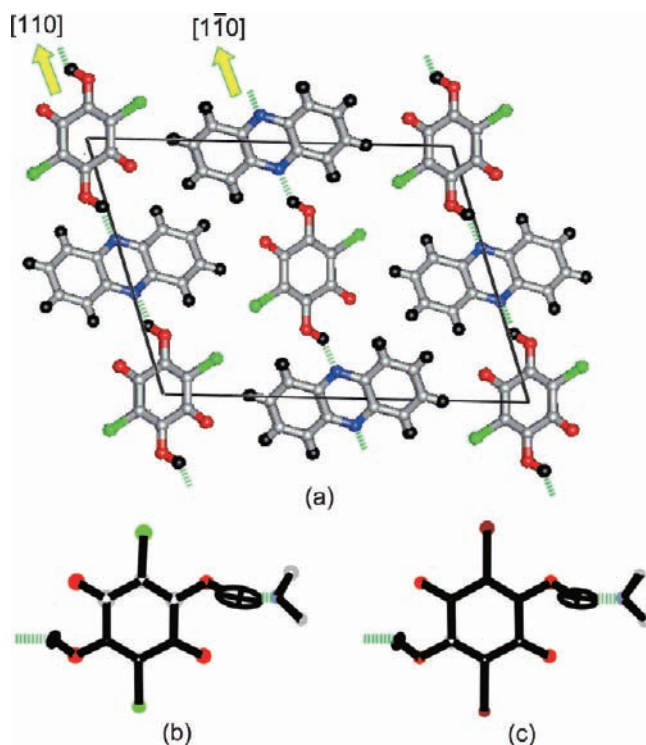
thermal change of pressure with 7.6×10^{-4} GPa/K (for $T > 90$ K) due to contraction of the medium.[17] The cooling and heating rate was 1−2 K/min, and the accuracy of temperature was ∼0.05 K.

2.3. High-Pressure X-ray Diffraction Studies. All the X-ray diffraction data at various temperatures were collected with a Rigaku DSC imaging plate system by using Si double-crystal monochromatized synchrotron radiation ($\lambda = 0.6877$ Å) at the beamlines BL-1A and BL-8A of Photon Factory (PF), High-Energy Accelerator Research Organization (KEK). The monochromatized beam is focused using a bent cylindrical mirror made of Si crystal coated with Rh, with a focused beam size of 0.3 (vertical) × 0.7 (horizontal) mm. The crystal attached on a glass fiber was cooled or heated by flowing helium or nitrogen gas in the case of ambient pressure measurement. High-pressure diffraction studies were conducted using a clamp-type high-pressure cell[18] filled with Daphne 7373 oil, and the cell was mounted at the cold head of a closed cycle He gas refrigerator. The pressure values at low temperature were calibrated by measuring the change in the lattice parameters of a NaCl single crystal.

3. RESULTS AND DISCUSSION

3.1. General Features of Phz-H_2xa (X = Cl, Br) at Ambient Pressure. For the background of the present research, let us briefly overview the previous studies on the dielectric, structural, and optical properties of the ferroelectric Phz-H_2xa (X = Cl, Br) cocrystals at ambient pressure.
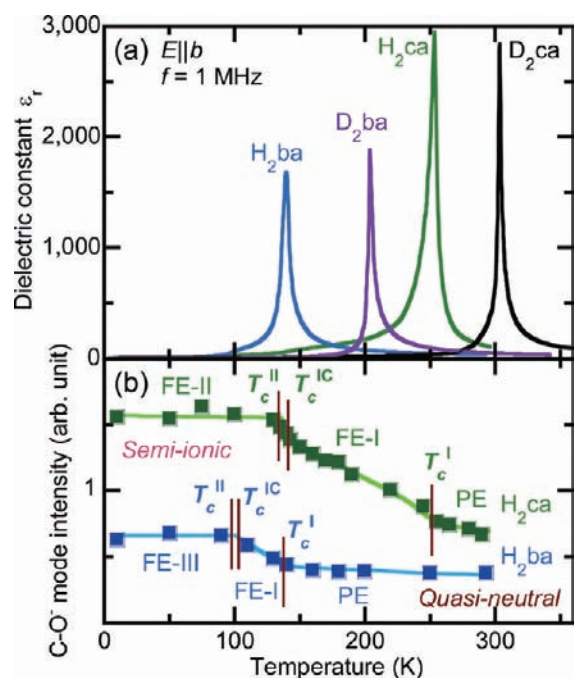
3.1.1. Molecular Packing. The Phz and H_2xa molecules construct the segregated $\pi−\pi$ stacking along the crystallographic b-direction of a monoclinic lattice (Figure 1). Along the

Figure 1. (a) The molecular packing with hydrogen bond (thick solid lines) viewed on the (010) plane. (b) The FE-I phase structure of Phz-H_2ca at 160 K and (c) Phz-H_2ba at 100 K showing the protons displacement from H_2xa to the C=N−C units of Phz moiety observed by the neutron diffraction.

[110] or [1̄10] direction, they are alternately linked side-by-side forming a linear chain by the intermolecular O−H···N bonds. Below the Curie point (T_c^I), the crystal symmetry is lowered from $P2_1/n$ to $P2_1$ in the space group, which yields a uniaxial polar axis along the b direction for ferroelectricity.

3.1.2. Ferroelectric Properties. The dielectric measurements along the (polar) *b*-direction exhibited a divergent increase of permittivity ε_r up to 2000–3000 at T_c^I (Figure 2a), and the ferroelectricity was proved with spontaneous polarization of
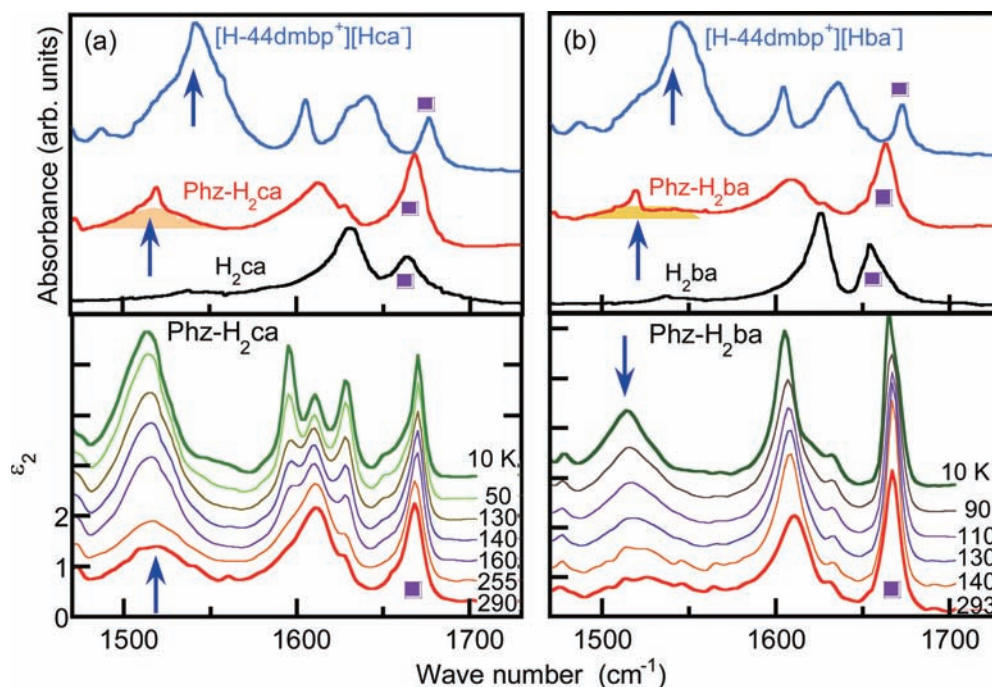
$1–2$ μC cm^{-2} by both the *P–E* hysteresis loop and pyroelectricity.[12] As shown below, we found the Curie–Weiss-like behavior without a sign of divergence indicative of antiferroelectric coupling, when the ac field *E* is approximately directed along the hydrogen-bonded chains: $E \perp (100)$ or $(10\bar{1})$ plane.

3.1.3. Successive Phase Transitions. The ferroelectric (FE-I) phase existing below T_c^I undergoes further two additional phase transitions at T_c^{IC} and T_c^{II}, as identified by the heat capacity measurements[19,20] and modest kink- or cusp-like anomalies of permittivity (see below). At T_c^{IC}, the system remains ferroelectric but appears as an incommensurate superlattice in a narrow temperature range, according to the X-ray diffraction studies.[12] This phase is called IC hereafter. Finally at T_c^{II}, this modulation vector immediately locks-in to a 2-fold periodicity for Phz-H_2ca and to a 3-fold one for Phz-H_2ba. Here we denote these lowest-temperature phases as FE-II and FE-III to distinguish the different lock-in periodicities, respectively.

3.1.4. Proton Displacive Ferroelectricity. The neutron diffraction studies on FE-I phase structures exhibited one acidic proton displacing to the middle position of the O···N bond (Figure 1b,c), and then the molecules appear to gain partially ionic ($O^{-}···H-N^{+}$) character compared with the high-temperature PE phase structure. The Phz-H_2ca crystal was found to be more ionic than Phz-H_2ba judging from the longer proton displacement by about 0.1 Å (Figure 1b,c).

3.1.5. Molecular Ionicity. The molecular ionicity (Figure 2b) has been also monitored by the mode intensity of $C-O^{-}$ stretch vibration around 1500–1550 cm^{-1} in the infrared spectra, because this absorption is absent for the neutral H_2xa but becomes prominent for the Hxa^{-} salts.[21] At room temperature, this band intensity is very weak for the Phz-H_2ca and Phz-H_2ba crystals and almost absent for the Phz-H_2fa crystal. Development of ionic character upon cooling is evident from previously reported data[21]

Figure 2. Temperature-dependent properties at ambient pressure. (a) Relative dielectric constant of Phz-H_2xa (X = Cl, Br) and their deuterated cocrystals measured along the crystallographic *b*-axis at $f = 1$ MHz. (b) Mode intensity of the charge-sensitive $C-O^{-}$ stretch vibration for Phz-H_2xa (X = Cl, Br) cocrystals.

Figure 3. Infrared spectra and their thermal evolutions of (a) Phz-H_2ca and (b) Phz-H_2ba. The absorption spectra of Phz-H_2xa powder in KBr disk (upper panels) are compared with those of neutral H_2xa and monovalent ionic Hxa^{-} species in 4,4dmbp (4,4′-dimethyl-2,2′-bipyridine) salts. The spectra on the single crystals (lower panels) at various temperatures are derived as the imaginary part of the *E*||*a* dielectric spectra ε_2 through the Kramers–Kronig transformation of reflectivity data. The absorption bands indicated by arrows (also with shaded area) and squares are ascribed to the $C-O^{-}$ and $C=O$ stretch vibrational modes, respectively.

on imaginary part ε_2 of the $E\|a$ dielectric spectra, as partially reproduced in Figure 3. The ionicity increases gradually in the FE-I phase upon cooling to the T_c^{IC}, below this temperature it becomes almost constant as shown in Figure 2b. For proton-transferred Hxa$^-$ ions, the C$-$O$^-$ stretch vibrational mode exhibits more than twice the intensity of the C$=$O stretch mode (see the spectra of [H-44dmbp$^+$][Hxa$^-$] in Figure 3). Judging from the comparable or lower C$-$O$^-$ stretch mode intensity relative to the C$=$O mode, both Phz-H$_2$ca and Phz-H$_2$ba are regarded as semi-ionic rather than fully ionic in the FE-I phase. The Phz-H$_2$ca exhibits stronger C$-$O$^-$ stretch band intensity than Phz-H$_2$ba, in agreement with the longer proton displacement in the FE-I structures (Figure 1b,c).
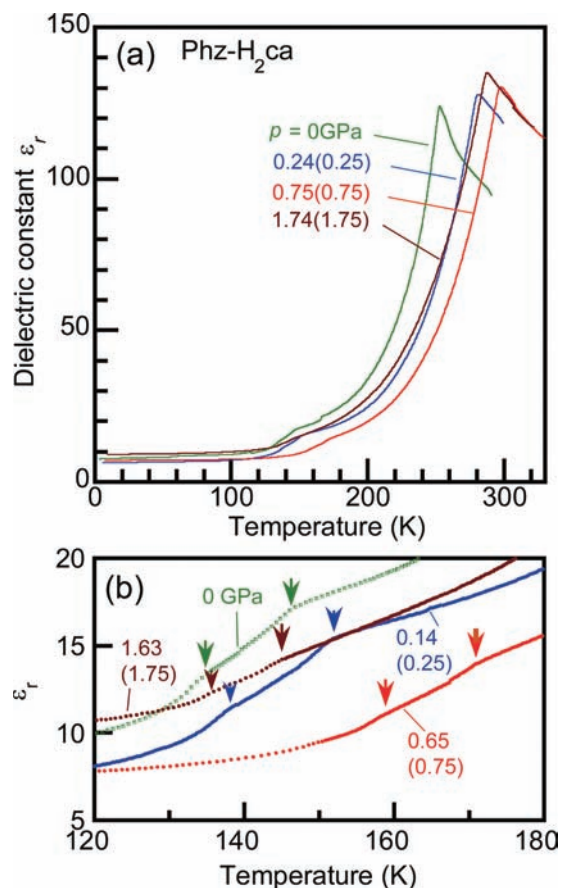
The C$-$O$^-$ vibrational mode intensity does not go up any more below the T_c^{II}, and then the semi-ionic character persists even in the FE-II or FE-III phases. Actually for Phz-H$_2$ca, the ^{35}Cl nuclear quadrupolar resonance (NQR) experiments by Kanoda et al. showed the preservation of averaged ionicity at T_c^{IC} and T_c^{II}.[22] Considering also the disordered nature of the displacing proton in the FE-I phase (see the anomalously elongated thermal ellipsoid in Figure 1c), the observed superlattice of the FE-II/III phases could be naturally related to the corresponding periodic order of this proton. This conjecture is also supported by the observation[19,20] that total transition entropy at T_c^{IC} and T_c^{II} is close to that expected for the order$-$disorder mechanism. In this picture, for instance, half of disordered protons would be back to more neutral O$-$H$\cdots$N form (N) and the rest forward to more ionic O$^-\cdots$H$-$N$^+$ form (I), and their alternating periodicity ($\cdots$N$-$I$-$N$-$I$\cdots$) is a likely origin of doubled superlattice of the FE-II phase.

3.2. High-Pressure Dielectric Properties of Phz-H$_2$xa (X = Cl, Br). Our earliest report included the temperature dependent b-axis dielectric constant under modest pressure; application of hydrostatic pressure up to 0.60 and 0.91 GPa for Phz-H$_2$ca and Phz-H$_2$ba, respectively, resulted in a monotonic increase of T_c^I. First, we examined the dielectric properties on three cocrystals of different Curie points T_c^I: Phz-H$_2$ca (T_c^I = 253 K), Phz-H$_2$ba (138 K), and deuterated Phz-D$_2$ba (204 K). The low-temperature anomalies of b-axis dielectric constant ε_r are often too obscured to clearly identify the T_c^{II} in the steep slope of ε_r-T curvature. Instead, the T_c^{IC} and T_c^{II} were easily identified by the kink anomalies of the data with ac field applied normal to the (10$\bar{1}$) plane for Phz-H$_2$ca and Phz-H$_2$ba (Figures 4 and 5a, respectively) or normal to the (100) plane for Phz-D$_2$ba (Figure 5b).

For the Phz-H$_2$ca crystal, all these anomalies likewise shift to the high temperature under 0.7 GPa and then gradually back to the lower temperature with pressure above 0.8 GPa (Figure 4). On the other hand for Phz-H$_2$ba and Phz-D$_2$ba crystals, the anomalies at T_c^{IC} and T_c^{II} showed the complicated changes, initially positive, then negative, and again positive temperature shifts with pressure, in contrast to the monotonous increase of T_c^I, as shown in Figure 5.

3.3. Pressure$-$Temperature Phase Diagram. Based on the dielectric properties shown above, we obtained the $p-T$ phase diagrams as summarized in Figure 6.

3.3.1. Phz-H$_2$ca. All the phase transition points steeply increase in the low-pressure region (dT_c^I/dp = +120 K/GPa and dT_c^{II}/dp = +50 K/GPa near 0 GPa) saturate at 0.6$-$0.8 GPa and then turn to gradual decrease with pressure. The phase diagram exhibits nearly parallel three curves of T_c^I, T_c^{IC}, and T_c^{II}, dividing the state into the PE, FE-I, IC, and FE-II phases (Figure 6a).
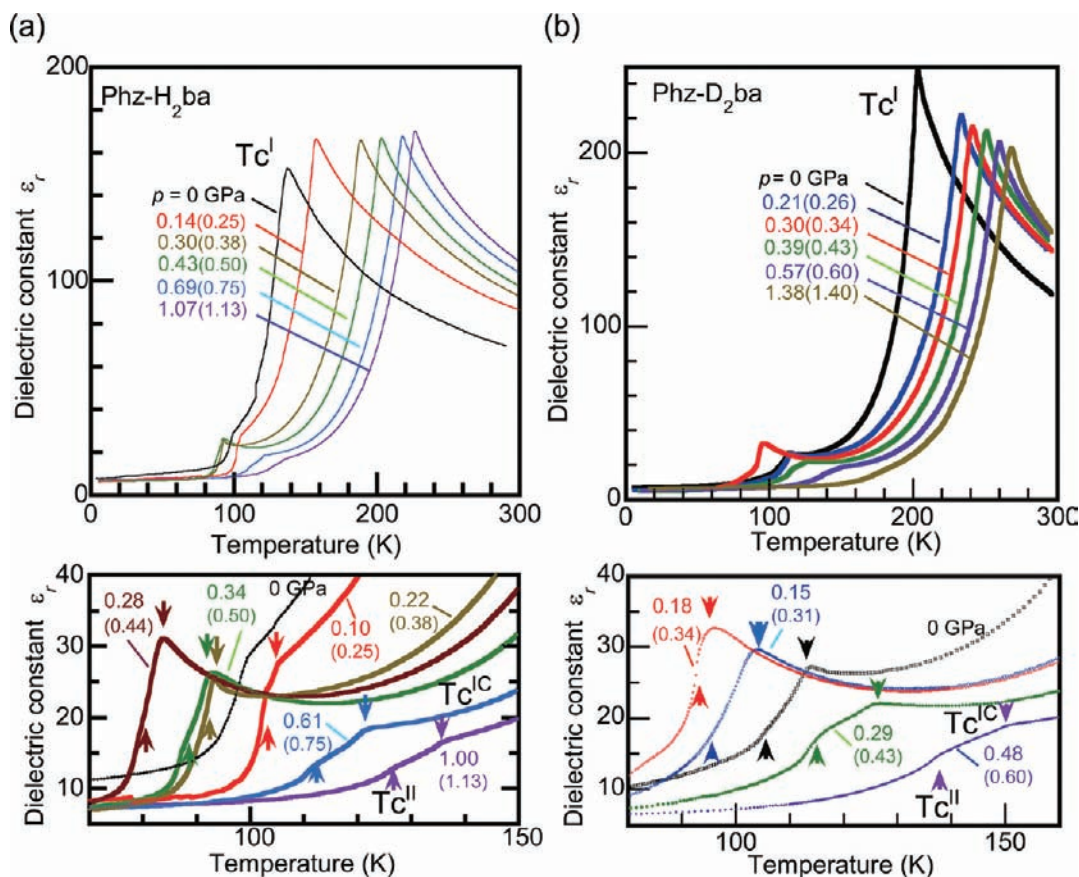

Figure 4. Temperature variation of relative dielectric constant of Phz-H$_2$ca under various pressures. The ac field (100 kHz) was applied normal to the (10$\bar{1}$) plane. Upper panel is the overall thermal change, and the lower panel magnifies the data around the phase transitions at T_c^{IC} with cusp-like anomalies and at T_c^{II} with modest kink-like anomalies marked by arrows. The hydrostatic pressures are corrected values at T_c^I in the upper panel and at T_c^{II} in the lower one. The values in parentheses represent the load pressure (in GPa).
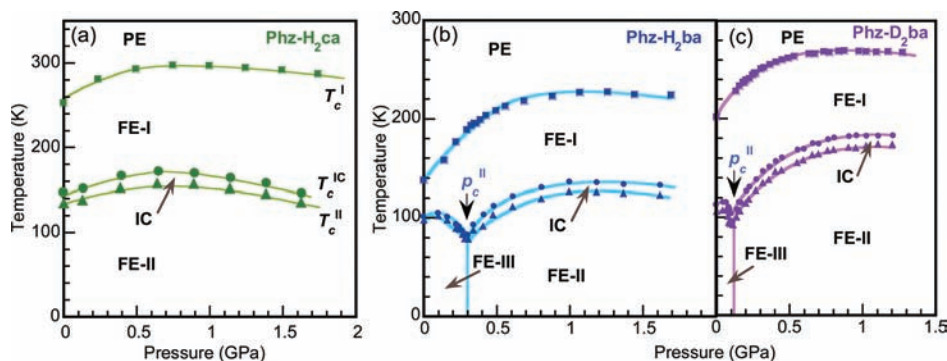
3.3.2. Phz-H$_2$ba and Phz-D$_2$ba. Both the Phz-H$_2$ba and deuterated Phz-D$_2$ba reveal the similar pressure-dependence of T_c^I: monotonic increase at low-pressure region and saturation at high pressures beyond ~1.0 GPa. The respective slopes of dT_c^I/dp = +180 and +200 K/GPa near p = 0 GPa are much higher than those of hydrogen-bonded ferroelectric KH$_2$PO$_4$ (KDP, $-$46 K/GPa) and its family ($-$14$\sim -$140 K/GPa);[23] this manifests high sensitivity to the pressure in this molecular compound family. The phase diagrams (Figure 6b,c) are more complicated in the low-p and -T region than that of Phz-H$_2$ca. The T_c^{IC} and T_c^{II} simultaneously decrease as showing sharp dips at pressures of p_c^{II} = 0.29 GPa for Phz-H$_2$ba and 0.11 GPa for Phz-D$_2$ba. This behavior suggests a new phase boundary, i.e., a vertical line at p_c^{II}.

The overall phase diagram of deuterated Phz-D$_2$ba well resembles that of Phz-H$_2$ba. They are superposed well with each other by applying an amplified temperature scale by a factor of 1.2 and a shift of 0.18 GPa on the latter $p-T$ diagram to match the critical pressures p_c^{II}. It should be noted that this temperature scaling factor agrees well with the observed deuteration effect on the Phz-H$_2$ca: T_c^I(D)/T_c^I(H) = 304/253 = 1.20 and T_c^{II}(D)/T_c^{II}(H) = 169/137 = 1.23.

3.4. High-Pressure Properties of Phz-H$_2$fa. In the fluorine-substituted isomorph Phz-H$_2$fa, the paraelectric neutral state is contrastively stable in the whole temperature range at

1039

dx.doi.org/10.1021/ja208113p | *J. Am. Chem. Soc.* 2012, 134, 1036$-$1046

Figure 5. Temperature variation of relative dielectric constant under various pressures for (a) Phz-H_2ba measured with ac field (100 kHz) applied normal to the $(10\bar{1})$ and for (b) Phz-D_2ba measured with ac field (100 kHz) applied normal to (100) plane. Upper panels are overall thermal changes. The lower panels magnify the data around the phase transitions at T_c^{IC} with cusp-like anomalies and at T_c^{II} with modest kink-like anomalies marked by arrows. The hydrostatic pressures are corrected values at T_c^{I} in the upper panels and at T_c^{II} in the lower ones.
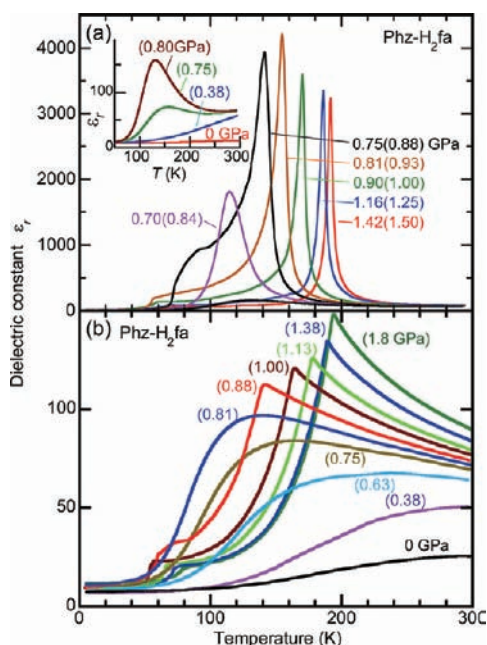

Figure 6. Temperature–pressure phase diagrams of (a) Phz-H_2ca, (b) Phz-H_2ba, and (c) Phz-D_2ba.

ambient pressure. Gradual increase of relative permittivity with temperature up to $\varepsilon_r \sim 25$ (at room temperature) for $E \perp (10\bar{1})$ indicates presence of some dipolar fluctuation and suggests a possible proximity to the ferroelectric instability.[12] This is why we anticipated possible emergence of ferroelectricity in this compound as well under hydrostatic pressure.

3.4.1. Dielectric Properties. As shown in the inset to Figure 7a, the *b*-axis permittivity markedly goes up with increasing pressure. At pressure of $p_c^{I} = 0.70$ GPa, the rounded maximum suddenly turns to a sharp peak at $T_c^{I} = 115$ K, indicative of pressure-induced phase transition. This observation is quite distinct from the quantum ferroelectricity, for which Curie point of the second-order transition continuously falls off toward

zero temperature (quantum critical point).[24] Therefore, this pressure-induced phase transition should be of the first order. Further compression rapidly increases the T_c^{I}. The divergently increasing ε_r value as high as 3000–4000 at T_c^{I} manifests the ferroelectricity with the *b*-direction polarity and is then similar to the cases of Phz-H_2ca and Phz-H_2ba.
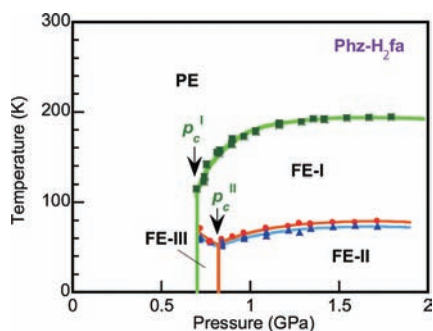
The anisotropic nature of dielectric properties was also examined by applying the ac electric field *E* perpendicularly to the crystallographic $(10\bar{1})$ plane, which lies approximately along the hydrogen-bonded chains. The rounded maximum of ε_r lying near room temperature is shifted to lower temperatures, and its height rapidly goes up with increasing load pressure from 0.1 MPa to 0.70 GPa. This anomaly suddenly changes to a

Figure 7. Temperature dependence of relative dielectric constant of the Phz-H_2fa crystal at various pressures. The hydrostatic pressures are corrected values at T_c^I. The values in parentheses represent the load pressure (in GPa). (a) The ac field (f = 100 kHz) was applied along the crystallographic b-axis and (b) normal to the $(10\bar{1})$ plane.

well-defined sharp peak characteristic of phase transition at critical pressure p_c^I. Beyond this pressure, the Curie−Weiss-like behavior without divergence at T_c^I indicates an antiferroelectric coupling along this direction. The pressure-induced ferroelectricity is concurrently accompanied by the additional low-temperature phase transitions as signified by the kink- or cusp-like anomalies. The temperature-dependence and anisotropic dielectric properties at pressures above p_c^I are very similar to those of other Phz-H_2xa (X = Cl, Br) ferroelectrics.

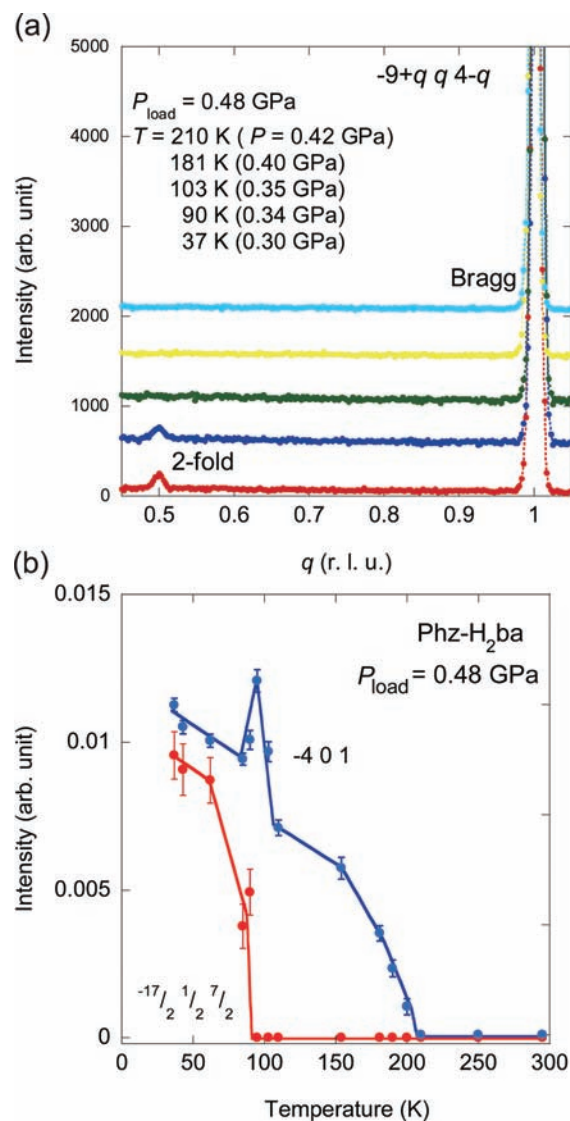*3.4.2. p−T Phase Diagram.* The T_c^{II} decreases first with pressure and is then minimized at p_c^{II} = 0.82 GPa. The phase diagram beyond this pressure is similar to that of Phz-H_2ba except that the maximum T_c^I is much lower. The T_c^I, T_c^{IC}, and T_c^{II} are finally saturated at 193, 79, and 74 K, respectively, under pressures above 1.3 GPa, exhibiting the upward bent curves in the phase diagram (Figure 8).

Figure 8. Temperature−pressure phase diagram of the Phz-H_2fa crystal.

3.5. High-Pressure X-ray Diffraction Studies. The synchrotron X-ray diffraction study has enabled us to identify the pressure-induced new phases for the Phz-H_2ba and Phz-H_2fa crystals.

3.5.1. Phz-H_2ba and Phz-D_2ba. At ambient pressure, both Phz-D_2ba and Phz-H_2ba crystals exhibit the modulation vector $\mathbf{q}$ = (1/3 ±1/3 0) for the ground state of FE-III phase. By applying hydrostatic pressure of 0.48 GPa (loaded at room temperature) on the Phz-H_2ba crystal, we found the different
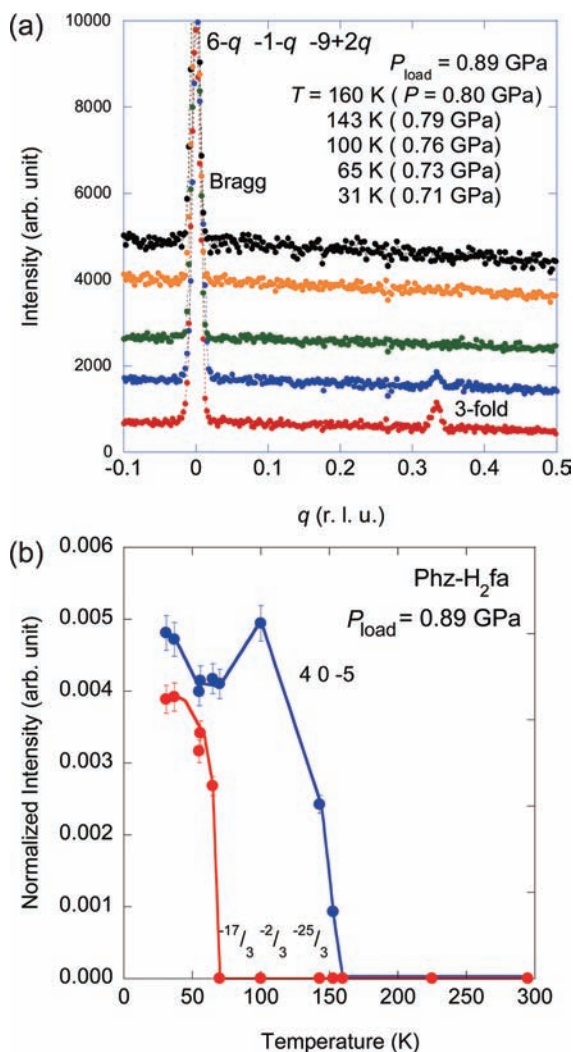

Figure 9. (a) X-ray diffraction profile of the Phz-H_2ba scanned along $(-9 + q\ q\ 4 - q)$ across the $(-8\ 1\ 3)$ reflection under hydrostatic pressure (P_{load} = 0.48 GPa) at various temperatures. The value in the parentheses represents the corrected pressure at measurement temperature, respectively. (b) Temperature dependence of peak intensity of the symmetry-breaking $(-4\ 0\ 1)$ reflection and 2-fold superlattice $(-17/2\ 1/2\ 7/2)$ reflection.

modulation. Figure 9a shows the temperature dependence of diffraction profile around $(-8\ 1\ 3)$ Bragg reflection scanned along $(hkl) = (-9 + q\ q\ 4 - q)$. At T = 37 K, the pressure was partly released to decrease to 0.30 GPa but still exceeded the p_c^{II}. Then, the crystal changes from the low-temperature FE-III to the new phase, and additional peak at $(-17/2\ 1/2\ 7/2)$ indicative of a 2-fold superlattice structure was clearly observed. Temperature dependence of the peak intensity indicates that the symmetry breaking peaks with $(h0l)$ ($h + l$ = odd) and $\mathbf{q}$ = (1/2 1/2 1/2) superlattice peak can be observed below T_c^I

and T_c^{II}, respectively, as shown in Figure 9b. The modulation vector $\mathbf{q} = (1/2\ 1/2\ 1/2)$ is identical to that of the Phz-H$_2$ca in the FE-II state. This identifies the pressure-induced change of the ground state from the FE-III to FE-II phase at p_c^{II}.
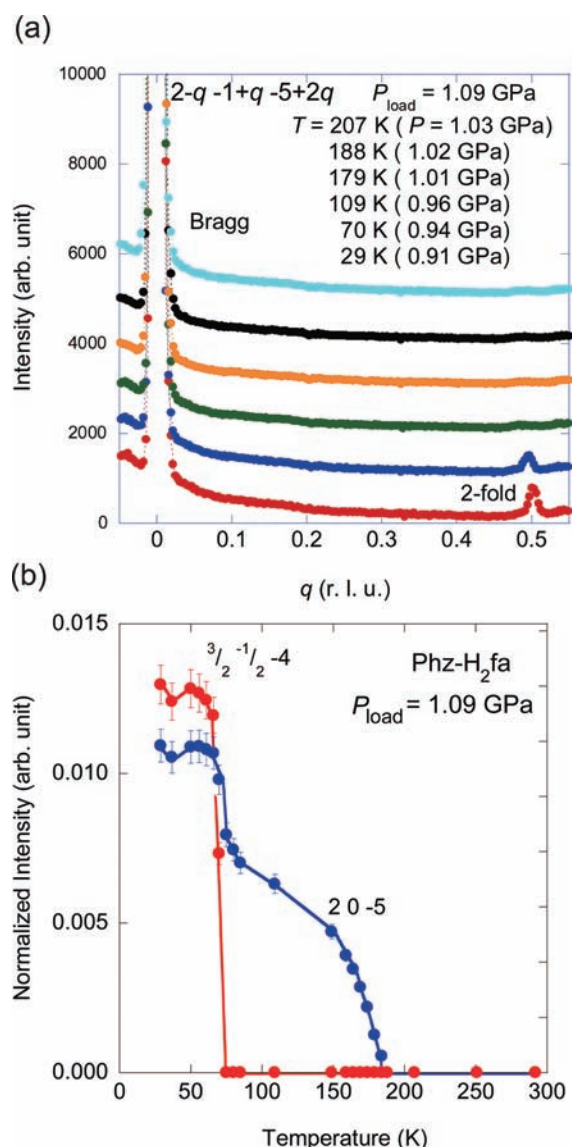
The peak intensity of the 2-fold peak was larger by 1 order of magnitude than that of 3-fold peak, which indicates much stronger structural modulation of the 2-fold periodicity in the FE-II state than that of the 3-fold one in the FE-III state.

3.5.2. Phz-H$_2$fa. High-pressure diffraction studies have confirmed the isomorphous structural change to the FE-I phase also for the Phz-H$_2$fa crystal; the symmetry is lowered into a monoclinic $P2_1$ structure with appearance of $(h0l)$ reflections $(h + l = \text{odd})$ at $T = 100$ K $(<T_c^I)$ under pressures of $p = 0.75$ and 0.95 GPa (Figures 10b and 11b). Figures 10a and 11a

Figure 10. (a) X-ray diffraction profile of the Phz-H$_2$fa scanned along $(6 - q\ -1 - q\ -9 + 2q)$ under hydrostatic pressure ($P_{\text{load}} = 0.89$ GPa) measured at various temperatures. The value in the parentheses represents the corrected pressure at measurement temperature, respectively. (b) Temperature dependence of peak intensity of the symmetry-breaking $(4\ 0\ -5)$ reflection and 3-fold superlattice $(-17/3\ -2/3\ -25/3)$ reflection.

show the diffraction profiles of Phz-H$_2$fa single crystal under the load pressure of 0.89 and 1.09 GPa, respectively. In the lower-pressure measurements (Figure 10a), the 3-fold periodicity was observed as shown by the appearance of new peak at
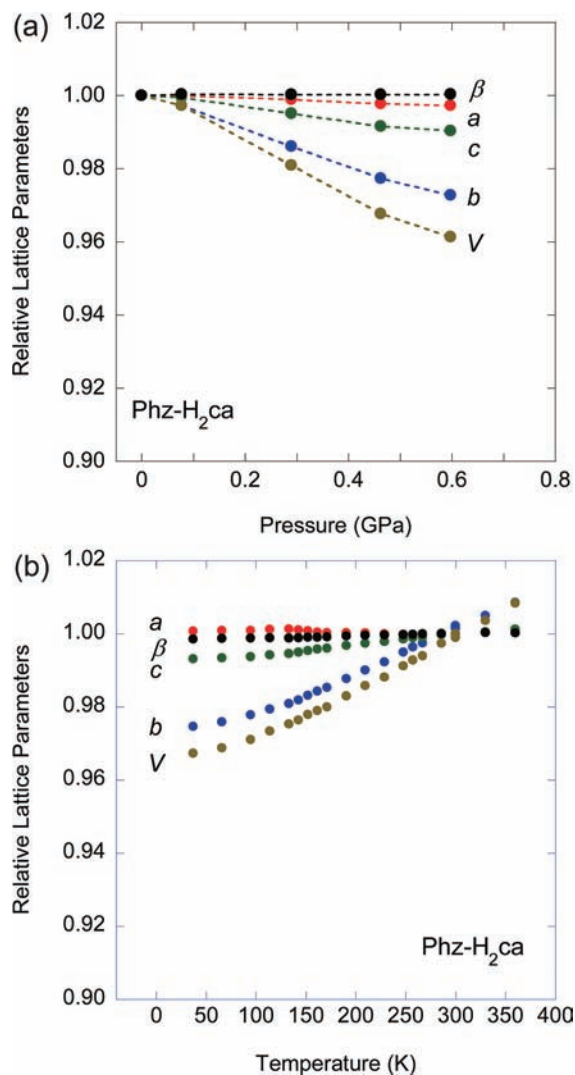

Figure 11. (a) X-ray diffraction profile of the Phz-H$_2$fa scanned along $(2 - q\ -1 + q\ -5 + 2q)$ under hydrostatic pressure ($P_{\text{load}} = 1.09$ GPa) measured at various temperatures. The value in the parentheses represents the corrected pressure at measurement temperature, respectively. (b) Temperature dependence of peak intensity of symmetry-breaking $(2\ 0\ -5)$ reflection and 2-fold superlattice $(3/2\ -1/2\ -4)$ reflection.

$(17/3\ 4/3\ -25/3)$ below T_c^{III}. On the other hand, one can find the 2-fold periodicity, as seen from the emergence of the new peak at $(3/2\ -1/2\ -4)$ below T_c^{II} under higher pressure measurements (Figure 11a). These 3- and 2-fold periodicities for the ground states have different modulation vectors from those of Phz-H$_2$ba and Phz-H$_2$ca crystals: $\mathbf{q} = (1/3\ 1/3\ 1/3)$ at $(p, T) = (0.70\ \text{GPa},\ 31\ \text{K})$ and $(1/2\ 1/2\ 0)$ at $(0.90\ \text{GPa},\ 29\ \text{K})$. The peak intensity of 2-fold modulation is larger than that of 3-fold one, as in the case of the Phz-H$_2$ba.

3.6. Lattice Compression Effect on Curie Point. The pressure-induced elevation of T_c^I is opposite to the case of conventional displacive-type ferroelectrics, in which the lattice hardening destabilizes the ferroelectric soft mode and reduces the Curie point.[25] This observation cannot be explained by the mechanism of simple proton-hopping between two equilibrium minima; the proton ordering becomes destabilized with
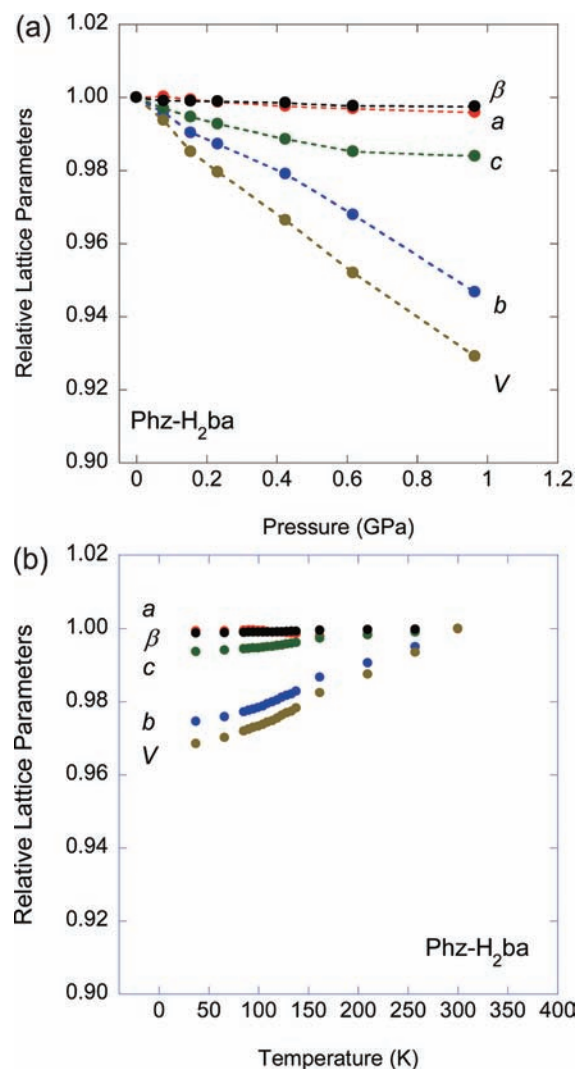
shrinkage of hydrogen bonds, as seen in the KDP family and squaric acid crystals. In fact, there is no apparent correlation between the T_c and O···N distance.[12]

The ferroelectric phase transition may be accounted for by competition between ionization energy and increased electrostatic gain of ionized lattice, as in the case for the NI transition. It is conjectured that the ionicity increases under hydrostatic pressure by increasing the attractive interactions between acid and base molecules in the ac plane, as shown in Figure 1a. To check this scenario, we examined the pressure dependence of lattice constants for each crystal. In the case of Phz-H$_2$ca

Figure 12. The lattice constants of the Phz-H$_2$ca single crystal normalized at ambient condition. (a) Pressure dependence at room temperature. (b) Temperature dependence at ambient pressure.

(Figure 12a), the a-axis, which is close to the hydrogen-bonded chain direction, exhibited a very small shrinking ratio. Although the c-axis shrinks with application of pressure, a tendency of saturation was observed in the high-pressure region. The T_c saturation at higher pressure might reflect the nonlinear lattice shrinkage of the c-axis. On the other hand, compressibility of b-axis, which is a π-stacking direction of identical molecules, is the largest. If the low-temperature FE phase had a fully ionic structure, the strongest Coulombic interaction would be repulsive between the same positive or negative charged molecules and then decrease the
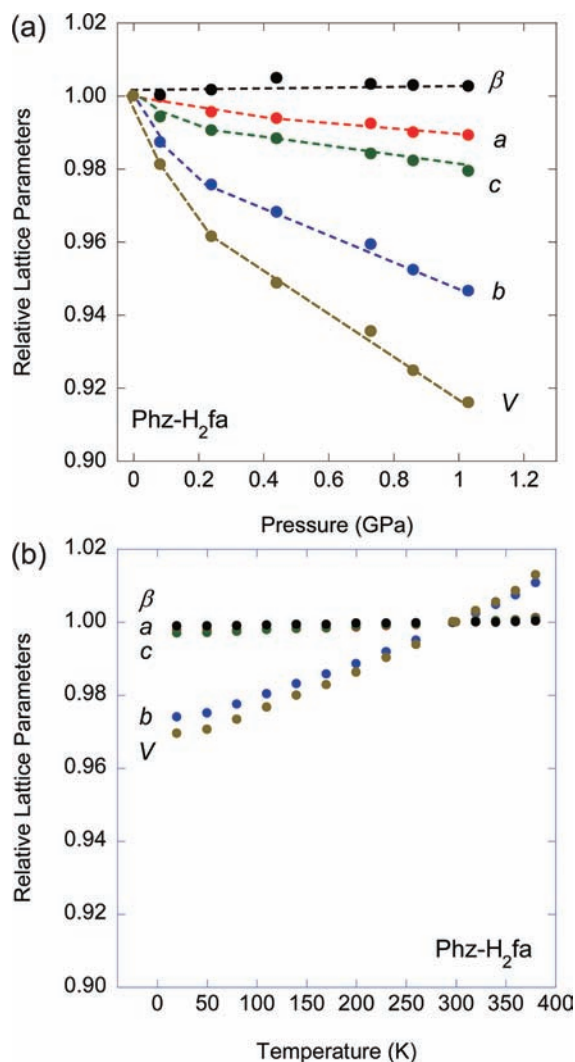

Figure 13. The lattice constants of the Phz-H$_2$ba single crystal normalized at ambient condition. (a) Pressure dependence at room temperature. (b) Temperature dependence at ambient pressure.

transition temperature. However, the observed opposite behavior to this expectation in the low-pressure regime suggests some reduced effect of the repulsion. The possible scenario can be the charge disproportionation, which is the origin of the pressure-induced semi-ionic state (vide infra). Furthermore, the saturation and slight decrease of T_c in the higher pressure regime can be understood by the competition between the compression in the attractive c-axis and the effect of repulsive effect in the b-axis direction. The pressure dependence of lattice constants of Phz-H$_2$ba or Phz-H$_2$fa crystal shows similar tendency (Figures 13a and 14a).

As shown in Figures 12b, 13b, 14b, the temperature dependences of lattice constants are small compared with their corresponding pressure dependences. For example, in the case of Phz-H$_2$fa (Figure 14b) the compressibility of lattice constant is less than 1% (a or c) or 3% (b) down to 20 K. These compressions correspond to the pressure effect of only 0.2−0.3 GPa. This would explain why the Phz-H$_2$fa exhibiting ferroelectricity under pressure beyond 0.70 GPa did not undergo the ferroelectric transition at ambient pressure.

3.7. Universal Phase Diagram. The above structural assignments have allowed us to depict a universal picture of the phase diagram, as shown in Figure 15. Whereas the Phz-H$_2$ca

Figure 14. The lattice constants of the Phz-H_2fa single crystal normalized at ambient condition. (a) Pressure dependence at room temperature. (b) Temperature dependence at ambient pressure.
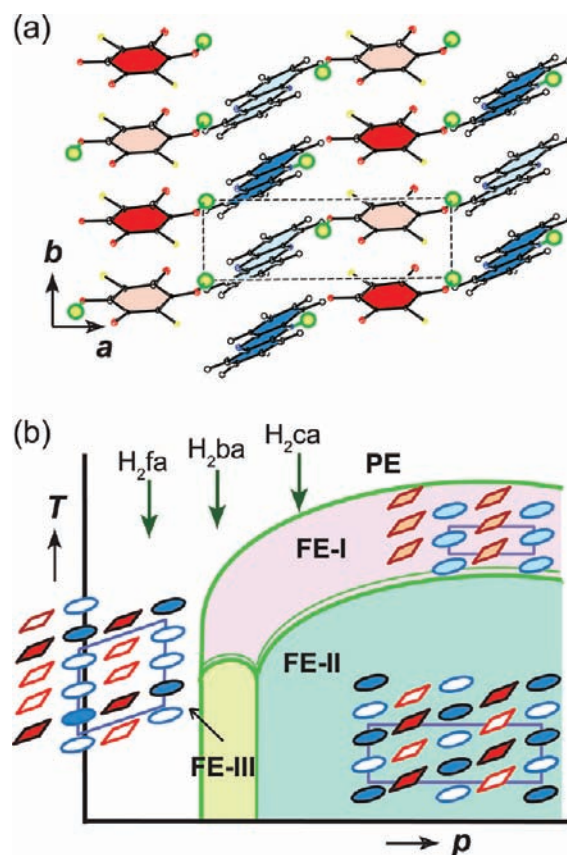
and Phz-H_2fa cocrystals are located at the highest and lowest sides of (hypothetical) pressure, respectively, the Phz-H_2ba is close to the boundary at p_c^I, which distinguishes between the PE ground state and a set of the FE-I, IC, and FE-III phases. The FE-III ground state is transformed to FE-II at the p_c^{II}, where T_c^{II} is minimized. That is, the ground state is successively changed from the PE to FE-II phase through the FE-III as the ferroelectricity is increasingly stabilized under compression.

To summarize the above, the hydrostatic pressure inclines to accelerate the proton-transfer reaction and realizes the more ionic ground state with stabilizing ferroelectricity in all the Phz-H_2xa crystals.

3.8. Possible Picture of Inhomogeneous Ionicity. Here we argue the origin and possible picture of the semi-ionic structures in the ferroelectric phases. The CT complexes have demonstrated homogeneous ionization during the NI transition, as is typically observed in the ferroelectric tetrathiafulvalene (TTF)-p-chloranil (CA)[26] and its antiferroelectric analogue, 4, 4′-dimethyltetrathiafulvalene (DMTTF)-CA.[27] Meanwhile, since the theoretical prediction by Hubbard and Torrance,[28] a periodic neutral ionic segregation or so-called staging lattice has been a subject of continued interest[29,30] that would be

expected from frustrated Coulomb interaction among ionized molecules below the NI transition temperature. Whereas the electrostatic forces are attractive along the DA-alternating stacks, they can be either repulsive or attractive between the neighboring stacks. If some interstack direction has enough strong repulsion, the D and A molecules can be segregated into relatively neutral and ionic species with periodic N−I−N−I order along this direction forming a stripe- (one-dimensional) or sheet-like (2-dimensional) pattern to relax this frustration. The 3,3′,5,5′-tetramethylbenzidine (TMB)−7,7,8,8-tetracyano-p-quinodimethane (TCNQ) complex has been thought to be the candidate based on its optical spectra, although the corresponding low-temperature structure has not been determined yet due to experimental difficulty, such as a crack occurring in its crystals.[31] According to theoretical calculations, these donor−acceptor (DA) molecular packing yields such a delicate balance between the attractive and repulsive Coulomb forces that stability of staging lattice depends even on the details of charge distribution on molecules. The staging lattices have not been fully identified yet and then remain as controversy.[32]

As compared with these cases, the segregated π-molecular stacking brings the clearer origin of Coulomb force frustrations in the Phz-H_2xa crystals. Figure 15a schematically depicts

Figure 15. (a) One-layer molecular packing viewed on the (001) plane with the model of neutral ionic segregation in the FE-II phase due to periodic ordering of protons (filled circles). (b) Schematic representations of the phase diagram for the series of Phz-H_2xa and of the neutral ionic charge distributions within a molecular layer. Neutral and ionic molecules are represented by the open and filled symbols (Phz = square, H_2xa = circle), respectively.

one-layer molecular arrangements (∥(001) plane) formed by the hydrogen-bond and π-stack interactions. Each stack of

protonated H-Phz$^+$ cations or deprotonated Hxa$^-$ anions must bear much stronger repulsive interactions on the nearest neighbor molecules with short separation of $b \sim 3.84–3.92$ Å compared with the possible interstack repulsions in the DA alternating CT complexes with much larger separations (>5 Å). Attractive interactions in the Phz-H$_2$xa work on the next-nearest molecules along the supramolecular chains and the interlayer c direction. Then, one can anticipate the N−I alternation order along the π-stack (crystallographic $b-$) direction; this is in agreement with the actual observations, as described below.

First we argue the possible charge distribution in the FE-II phase of the Phz-H$_2$ca and pressurized Phz-H$_2$ba crystals. With the modulation wave vector $\mathbf{q} = (1/2\ 1/2\ 1/2)$ and preserved $2/m$ Laue symmetry, the 2-fold primitive superlattice can be further doubled in volume for a C-centered monoclinic lattice, as related by $(\mathbf{a}', \mathbf{b}', \mathbf{c}') = (-2\mathbf{a}, -2\mathbf{b}, \mathbf{a} + \mathbf{c})$ with the FE-I structure. The space group $C1$ is deduced from the polar nature and just a subgroup symmetry of the FE-I structure ($P2_1$). Similarly, $\mathbf{q} = (1/2\ 1/2\ 0)$ for the pressurized Phz-H$_2$fa crystal corresponds to the similar C-centered monoclinic lattice $(\mathbf{a}', \mathbf{b}', \mathbf{c}') = (2\mathbf{a}, 2\mathbf{b}, \mathbf{c})$ having the same periodicity within a molecular layer but the different interlayer relationship. Such symmetry poses homogeneous ionicity within each hydrogen-bonded chain but can cause the alternation in the ionicity as the N−I−N−I sequence along the π-molecular stack, as schematized in Figure 15a. This alternation can most effectively release the strongest Coulomb repulsions in the above frustrated lattice and then is the most likely structure of the FE-II phase. Likewise, the N−N−I-type alternation along the π-stacking columns shown in Figure 15b can commonly elucidate both modulation vectors $\mathbf{q} = (1/3\ \pm1/3\ 0)$ and $(1/3\ 1/3\ 1/3)$ for the FE-III superstructures with a only difference in the interlayer relations from that of FE-II.

4. CONCLUSION

The ferroelectricity of present supramolecular system has been closely related to acid−base chemistry, and the stability of neutral or semi-ionic ground state reflects the relative proton affinities of component molecules. Another characteristic of neutral ionic valence instability is a high sensitivity to the applied hydrostatic pressure, which can effectively change the intermolecular electrostatic interactions of ionized molecules. The systematic studies of materials have revealed a universal picture of pressure−temperature phase diagram involving various structural phases. The Phz-H$_2$fa crystal exhibits the critical pressure p_c^{I} distinguishing between the neutral paraelectric and the semi-ionic ferroelectric phases. Under pressure applied beyond the p_c^{I}, the Phz-H$_2$fa and Phz-H$_2$ba crystals unravel another critical pressure p_c^{II} changing the superlattice periodicity of the ground states. The strong repulsive Coulomb interactions along the π-molecular stack are responsible for such semi-ionic nature and superlattice formation of ferroelectric phases.

The anisotropic character of intermolecular electrostatic interactions will open new avenues on the supramolecular ferroelectrics. Versatile phase controls can be done by using a controlling parameters other than hydrostatic pressure. Because the Phz-H$_2$ba locates just over the p_c^{I} in the universal $p−T$ diagram, uniaxial shrinkage along the electrostatically repulsive b-direction would destabilize the semi-ionic ferroelectric phases and revive the para-electric ground states as a reverse effect to the pressurization. Ferroelectricity with different proton-transfer type NI transition can be also anticipated in supramolecular compounds other than the Phz-H$_2$xa cocrystals. For instance, ionicity change between neutral and ionic states could be more significant, if the π-molecular stacking has less Coulomb force frustration, like the DA alternating type of CT complexes.

■ AUTHOR INFORMATION

Corresponding Author

reiji.kumai@kek.jp

■ REFERENCES

(1) Oganov, A. R.; Chen, J.; Gatti, C.; Ma, Y.; Ma, Y.; Glass, C. W.; Liu, Z.; Yu, T.; Kurakevych, O. O.; Solozhenko, V. L. *Nature* **2009**, *457*, 863−867.

(2) Edwards, B.; Ashcroft, N. W. *Nature* **1997**, *388*, 652−654.

(3) Pickard, C. J.; Needs, R. J. *Nat. Mater.* **2008**, *7*, 775−779.

(4) Katrusiak, A.; Katrusiak, A. *Org. Lett.* **2003**, *5*, 1903−1905.

(5) Torrance, J. B.; Girlando, A.; Mayerle, J. J.; Crowley, J. I.; Lee, V. Y.; Batail, P.; LaPlaca, S. J. *Phys. Rev. Lett.* **1981**, *47*, 1747−1750.

(6) McConnell, H. M.; Hoffman, B. M.; Metzger, R. M. *Proc. Nat. Acad. Sci. U.S.A.* **1965**, *53*, 46−50.

(7) Metzger, R. M.; Torrance, J. B. *J. Am. Chem. Soc.* **1985**, *107*, 117−121.

(8) Koshihara, S.; Takahashi, Y.; Sakai, H.; Tokura, Y.; Luty, T. *J. Phys. Chem. B* **1999**, *103*, 2592−2600.

(9) Okamoto, H.; Ishige, Y.; Tanaka, S.; Kishida, H.; Iwai, S.; Tokura, Y. *Phys. Rev. B* **2004**, *70*, 165202.

(10) Horiuchi, S.; Tokura, Y. *Nat. Mater.* **2008**, *7*, 357−366.

(11) Horiuchi, S.; Ishii, F.; Kumai, R.; Okimoto, Y.; Tachibana, H.; Nagaosa, N.; Tokura, Y. *Nat. Mater.* **2005**, *4*, 163−166. *Nat. Mater.* **2008**, *7*, 922 (corrigendum).

(12) Horiuchi, S.; Kumai, R.; Tokura, Y. *J. Mater. Chem.* **2009**, *19*, 4421−4434.

(13) Kumai, R.; Horiuchi, S.; Sagayama, H.; Arima, T.; Watanabe, M.; Noda, Y.; Tokura, Y. *J. Am. Chem. Soc.* **2007**, *129*, 12920−12921.

(14) Perrin, D. D. *Dissociation Constants of Organic Bases in Aqueous Solution*; Butterworths: London, 1965; supplement, 1972.

(15) Wallenfels, K.; Friedrich, K. *Chem. Ber.* **1960**, *93*, 3070−3082.

(16) Horiuchi, S.; Kumai, R.; Tokura, Y. *J. Am. Chem. Soc.* **2005**, *127*, 5010−5011.

(17) Murata, K.; Yoshino, H.; Yadav, H. O.; Honda, Y.; Shirakawa, N. *Rev. Sci. Instrum.* **1997**, *68*, 2490−2493.

(18) Hasegawa, T.; Kumai, R.; Takahashi, Y.; Tokura, Y. *Rev. Sci. Instrum.* **2005**, *76*, 073903.

(19) Saito, K.; Amano, M.; Yamamura, Y.; Tojo, T.; Atake, T. *J. Phys. Soc. Jpn.* **2006**, *75*, 033601.

(20) Amano, M.; Yamamura, Y.; Sumita, M.; Yasuzuka, S.; Kawaji, H.; Atake, T.; Saito, K. *J. Chem. Phys.* **2009**, *130*, 034503.

(21) Fujioka, J.; Horiuchi, S.; Kida, N.; Shimano, R.; Tokura, Y. *Phys. Rev. B* **2009**, *80*, 125134.

(22) Kanoda, K.; Miyagawa, K.; Otani, M.; Iwase, F. unpublished.

(23) Srinivasan, M. R.; Shashikala, M. N.; Bhat, H. L. *Phase Trans.* **1991**, *35*, 205−242.

(24) Samara, G. A. *Phys. Rev. Lett.* **1971**, *27*, 103−106.

(25) Samara, G. A.; Sakudo, T.; Yoshimitsu, K. *Phys. Rev. Lett.* **1975**, *35*, 1767−1769.

(26) Tokura, Y.; Koda, T.; Saito, G.; Mitani, T. *J. Phys. Soc. Jpn.* **1984**, *53*, 4445−4455.

(27) Horiuchi, S.; Okimoto, Y.; Kumai, R.; Tokura, Y. *J. Am. Chem. Soc.* **2001**, *123*, 665−670.

(28) Hubbard, J.; Torrance, J. B. *Phys. Rev. Lett.* **1981**, *47*, 1750−1753.

(29) Bruinsma, R.; Bak, P.; Torrance, J. B. *Phys. Rev. B* **1983**, *27*, 456−466.

(30) Iwasa, Y.; Watanabe, N.; Koda, T.; Saito, G. *Phys. Rev. B* **1993**, *47*, 2920−2923.

(31) Buron-Le Cointe, M.; Lemée-Cailleau, M. H.; Cailleau, H.; Toudic, B.; Moréac, A.; Moussa, F.; Ayache, C.; Karl, N. *Phys. Rev. B* **2003**, *68*, 064103.

(32) Iizuka-Sakano, T.; Kawamoto, T.; Shimoi, Y.; Abe, S. *Phys. Rev. B* **2004**, *70*, 085111.